

**Fig. 4.**  $G(V_{sd}, B)$  for a 2- $\mu\text{m}$ -long tunnel junction at low  $B$ . A smoothed background has been subtracted to emphasize sharp features, although these are quite clear in the raw data. Oscillations are seen off the dispersion curves, several of which are easy to see.

dip. These last two effects are of particular interest because both the separation of spin and charge and the suppression of tunneling near  $V_{sd} = 0$  are hallmarks of Luttinger-liquid behavior (3).

It is interesting to find what limits the conservation of momentum in the experiment and how this shows up in the measurement. Clearly, any mechanism that breaks invariance to translations relaxes the constraint of momentum conservation and with it the conditions for allowing current to flow through the junction. Because of the high quality of CEO wires, momentum relaxation is mainly caused by the finite length of the tunnel junction.

The effects of finite size on  $G(V_{sd}, B)$  are very clear in the measurement of a 2- $\mu\text{m}$  tunnel junction. Figure 4 shows a zoom into the low  $B$  part of such a scan. Even for such a short junction, one can see the dispersions of the wires. On the other hand, contrary to the scan of the 6- $\mu\text{m}$  junction in Fig. 3,  $G(V_{sd}, B)$  is appreciable off the dispersions. One can see that the deviations of  $G(V_{sd}, B)$  from zero form a checkerboard pattern. This pattern is a striking manifestation of the finiteness of  $L$ : The momentum  $\delta$  function (that traces out the dispersion curves) oscillates as a function of its argument on a scale  $L^{-1}$ ; for a 6- $\mu\text{m}$  junction, periods that are one-third of the periods in Fig. 4 are observed. By viewing the checkerboard as Aharonov-Bohm oscillations, it is easy to show that the periods in the  $V_{sd}$  and  $B$  directions are indeed given by  $\Delta V_{sd} L / v_p = \Delta B L d = \phi_0$ , where  $\phi_0 = h/e$  is the flux quantum. This result can be also derived from a Fermi-liquid microscopic model (30). Similar oscillations appear in calculations that take interactions into account (31, 32).

**References and Notes**

1. P. Nozières, *Theory of Interacting Fermi Systems, The Advanced Book Program* (Addison-Wesley, Reading, MA, ed. 2, 1997).  
 2. B. L. Altshuler, A. G. Aronov, in *Electron-Electron Inter-*

*action in Disordered Systems*, A. L. Efros, M. Pollak, Eds. (North-Holland, Amsterdam, 1985), pp. 1–153.  
 3. V. J. Emery, in *Highly Conducting One-Dimensional Solids*, J. T. Devreese, R. P. Evrard, V. E. van Doren (Plenum, New York, 1979), pp. 247–303.  
 4. D. Yue, L. I. Glazman, K. A. Matveev, *Phys. Rev. B* **49**, 1966 (1994).  
 5. Y. Oreg, A. M. Finkel’stein, *Phys. Rev. B* **54**, R14265 (1996).  
 6. R. de Picciotto, H. L. Stormer, L. N. Pfeiffer, K. W. Baldwin, K. W. West, *Nature* **411**, 51 (2001).  
 7. D. L. Maslov, M. Stone, *Phys. Rev. B* **52**, 5539 (1995).  
 8. D. L. Maslov, *Phys. Rev. B* **52**, 14368 (1995).  
 9. I. Safi, H. J. Schulz, *Phys. Rev. B* **52**, 17040 (1995).  
 10. V. V. Ponomarenko, *Phys. Rev. B* **52**, 8666 (1995).  
 11. Y. Imry, *Introduction to Mesoscopic Physics* (Oxford Univ. Press, Oxford, 1997).  
 12. O. M. Auslaender et al., *Phys. Rev. Lett.* **84**, 1764 (2000).  
 13. T. Kleimann, M. Sassetti, B. Kramer, A. Yacoby, *Phys. Rev. B* **62**, 8144 (2000).  
 14. M. Bockrath et al., *Nature* **397**, 598 (1999).  
 15. H. W. C. Postma, T. Teepe, Z. Yao, M. Grifoni, C. Dekker, *Science* **293**, 76 (2001).  
 16. R. Goñi et al., *Phys. Rev. Lett.* **67**, 3298 (1991).  
 17. M. Sassetti, B. Kramer, *Phys. Rev. Lett.* **80**, 1485 (1998).  
 18. L. N. Pfeiffer et al., *Microelectron. J.* **28**, 817 (1997).  
 19.  $G$  is measured at  $T = 0.25$  K with standard lock-in techniques, in which a fixed excitation voltage of 10  $\mu\text{V}$  is applied at a frequency of 14 Hz.  
 20. A. Yacoby, H. L. Stormer, K. W. Baldwin, L. N. Pfeiffer, K. W. West, *Solid State Commun.* **101**, 77 (1997).  
 21. R. de Picciotto et al., *Phys. Rev. Lett.* **85**, 1730 (2000).  
 22. J. P. Eisenstein, L. N. Pfeiffer, K. W. West, *Appl. Phys. Lett.* **58**, 1497 (1991).

23. W. Kang, H. L. Stormer, L. N. Pfeiffer, K. W. Baldwin, K. W. West, *Nature* **403**, 59 (2000).  
 24. Being coplanar with the 2DEG, the only influence of  $B$  on it is by the Zeeman effect. This effect is negligible in GaAs in the  $B$  range that we use.  
 25. D. Carpentier, C. Peça, L. Balents, preprint available at xxx.lanl.gov/abs/cond-mat/0103193.  
 26. U. Zülicke, M. Governale, preprint available at xxx.lanl.gov/abs/cond-mat/0105066.  
 27. The densities that we find for the QWR are  $n_{uj} = 95 \pm 1$ ,  $68 \pm 1$ , and  $64.9 \pm 0.8 \mu\text{m}^{-1}$ , and those for the LQWR are  $n_{lj} = 92 \pm 1$ ,  $50.9 \pm 0.8$ ,  $36.9 \pm 0.9$ ,  $29 \pm 1$ , and  $21.6 \pm 0.9 \mu\text{m}^{-1}$ .  
 28. The densities with  $m^* = 0.75$  m are  $n_{uj} = 99 \pm 1$ ,  $68 \pm 1$ , and  $65.6 \pm 0.8 \mu\text{m}^{-1}$  and  $n_{lj} = 95 \pm 1$ ,  $50.9 \pm 0.8$ ,  $37.2 \pm 0.9$ ,  $29 \pm 1$ , and  $21.0 \pm 0.9 \mu\text{m}^{-1}$ .  
 29. We attribute the weakness of the interactions to screening by the 2DEG. In fact, the screening length, the width of the wires, and the spacing between them are on the same length scale.  
 30. O. E. Raichev, P. Vasilopoulos, *J. Phys. Cond. Mat.* **12**, 6859 (2000).  
 31. M. Sassetti, B. Kramer, personal communication.  
 32. D. Boese, M. Governale, A. Rosch, U. Zülicke, *Phys. Rev. B* **64**, 085315 (2001).  
 33. This work is the result of a long-term and fruitful collaboration with H. Stormer. Illuminating discussions with L. Balents, B. Kramer, and M. Sassetti have been very beneficial to us. We also thank B. Halperin, Y. Oreg, A. Stern, and U. Zülicke for helpful conversations. This work is supported by the U.S.-Israel Binational Science Foundation and by a research grant from the Fusfeld Research Fund. O.M.A. is supported by a grant from the Israeli Ministry of Science.

14 September 2001; accepted 19 December 2001

# Mapping the One-Dimensional Electronic States of Nanotube Peapod Structures

D. J. Hornbaker,<sup>1</sup> S.-J. Kahng,<sup>1\*</sup> S. Misra,<sup>1</sup> B. W. Smith,<sup>2</sup> A. T. Johnson,<sup>3,4</sup> E. J. Mele,<sup>3,4</sup> D. E. Luzzi,<sup>2,4</sup> A. Yazdani<sup>1†</sup>

Arrays of  $C_{60}$  molecules nested inside single-walled nanotubes represent a class of nanoscale materials having tunable properties. We report electronic measurements of this system made with a scanning tunneling microscope and demonstrate that the encapsulated  $C_{60}$  molecules modify the local electronic structure of the nanotube. Our measurements and calculations also show that a periodic array of  $C_{60}$  molecules gives rise to a hybrid electronic band, which derives its character from both the nanotube states and the  $C_{60}$  molecular orbitals.

Single-walled carbon nanotubes (SWNTs) have inspired remarkable advances in science and engineering at the nanometer scale during the past decade (1). For electronic applications, the SWNT appears to be an ideal template for fabricating single-molecule-

based devices, such as nanotube-based diodes (2–4), single-electron transistors (5, 6), memory elements (7), and logic circuits (8, 9). Due to their size and geometry, SWNTs also provide a unique opportunity for nanoscale engineering of novel one-dimensional (1D) materials systems, created by self-assembly of atoms or molecules inside the SWNT’s hollow core (10). The promise of this material synthesis method has been demonstrated recently by the discovery (11) and subsequent high-yield production (12) of  $C_{60}@SWNT$ : a supramolecular assembly resembling a nanoscopic peapod composed of a 1D array of  $C_{60}$  molecules nested inside a SWNT (Fig. 1A). The composite nature of  $C_{60}@SWNT$  peapods, as well as other simi-

<sup>1</sup>Department of Physics and Frederick Seitz Materials Research Laboratory, University of Illinois at Urbana-Champaign, Urbana, IL 61801, USA. <sup>2</sup>Department of Materials Science and Engineering, <sup>3</sup>Department of Physics and Astronomy, <sup>4</sup>Laboratory for Research on the Structure of Matter, University of Pennsylvania, Philadelphia, PA 19104, USA.

\*Present address: Department of Physics, Soongsil University, Seoul, Korea.  
 †To whom correspondence should be addressed. E-mail: ayazdani@uiuc.edu

lar structures (13), raises the exciting possibility of a nanoscale material having a tunable structure that can be tailored to a particular electronic functionality. However, other than structural characterization (12–16), little is known about these composite systems. In particular, it is unclear to what extent their electronic properties (17) are different or derived from those of the constituent parts—an issue that may affect the future design of similar hybrid nanostructures and their application in electronic circuits.

Here we report measurements made with a scanning tunneling microscope (STM) of the electronic states of individual  $C_{60}$ @SWNT peapods; and, together with theoretical modeling, we demonstrate several key electronic phenomena in this hybrid structure. For example, we show that the local electronic properties of SWNTs can be selectively modified by the encapsulation of a single  $C_{60}$  molecule. Moreover, we demonstrate that periodic arrangements of encapsulated  $C_{60}$  molecules give rise to new electronic bands derived from the interaction between  $C_{60}$  molecular orbitals and the SWNT band structure, presenting the possibility of designing hybrid structures in which an encapsulated molecule is used to define on-tube electronic devices. Furthermore, controlled periodic arrangements of encapsulated molecules can make it possible to create 1D resonant quantum structures that can be coupled via the unperturbed sections of the SWNT. Our experiments and theoretical calculations suggest that encapsulation provides additional means of control over the electronic states of SWNTs, which are already at the heart of many proposed approaches to nanoelectronics (1–9).

We performed our experiments using a home-built STM operating under ultrahigh vacuum (UHV) and cooled to  $\sim 4$  K by means of thermal coupling to a liquid helium bath. STM imaging of samples after processing (18) and cooling shows regions typical of an ordered Au(111) surface and other regions covered with isolated or bundled SWNTs. The images of many of the nanotubes revealed typical electronic modulations associated with the atomic lattice of pristine SWNTs (19, 20). However, about 10 to 20% of the SWNTs examined exhibited distinct electronic features in both imaging and spectroscopy measurements that identified them as peapods (Fig. 1A).

The characteristic feature of peapods appears in the STM images when we map their unoccupied electronic states, using positive sample biases exceeding about +1 V (Fig. 1B), whereby “peaks” appear to be superimposed on the atomic corrugation of the SWNT cage. Scanning along the top of the peapod, these peaks appear in STM topographs as periodic modulations having an amplitude of 0.3 to 0.5 Å, which is significantly larger than those due to the atomic

corrugations ( $\sim 0.1$  Å) (Fig. 1D). Examining many tubes, we found nine peapods that displayed ordered arrays of peaks, as many as several dozen, with an average spacing of 10.5 Å (with a SD of 1.0 Å). We also observed peapods with arrays containing spaces or “vacancies.” In contrast to the distinct periodic pattern observed in the unoccupied electronic states of peapods (Fig. 1B), STM topographs of their occupied electronic states show only features associated with the underlying atomic lattice of the SWNT cage (Fig. 1C).

The spatial period of the peaks in the peapods’ unoccupied electronic states matches closely the 10 Å average spacing in close-packed arrays of the  $C_{60}$  molecules measured with transmission electron microscopy (TEM) at room temperature (Fig. 1A) (12, 14). Hence, we associate these periodic features with chains of encapsulated  $C_{60}$  molecules, and we associate their interaction with

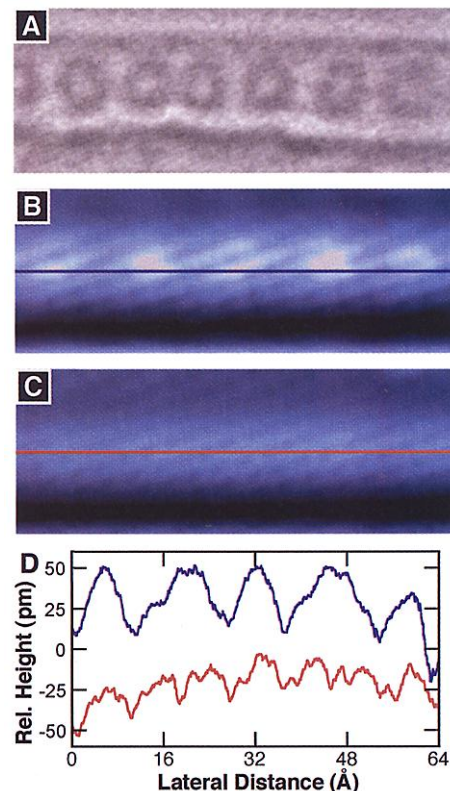


**Fig. 1.** Structure and STM imaging of a peapod. (A) A room temperature TEM image (105 Å by 29 Å) of a peapod, showing the SWNT cage and encapsulated  $C_{60}$  molecules. (B) STM image (105 Å by 29 Å) of a peapod obtained under positive sample bias (+1.5 V, 700 pA) showing both atomic corrugation of the SWNT and features associated with the encapsulated  $C_{60}$  molecules. (C) An image of the same peapod with a negative bias (-1.5 V, 700 pA) shows only the atomic corrugation of the SWNT. (D) Comparison of the apparent corrugation of positive (blue) and negative (red) bias STM line scans measured along the top of the peapod [corresponding lines are shown in (B) and (C)].

the nanotube cage. More important, contrasting the occupied and the unoccupied maps of the electronic states, we conclude that the interactions between the  $C_{60}$  molecules and the nanotube cage do not alter the nanotube’s atomic lattice, which is consistent with theoretical calculations that predict the encapsulation process to be energetically most favorable when it does not create structural distortion in the SWNTs (17). It is also consistent with TEM experiments providing evidence for weak van der Waals bonding between the  $C_{60}$  molecules and the SWNT cage by demonstrating that the  $C_{60}$  molecules are mobile inside the peapods at room temperature (12, 16). Overall, examination of the STM images of individual peapods leads us to conclude that although the interior fullerenes do not affect the atomic structure of the SWNT cage, they do modify its electronic states.

Previous STM spectroscopy has shown that unfilled SWNTs exhibit densities of states (DOSs) indicative of 1D metals or semiconductors, with the onset of subbands at successively higher energies (19, 20). All the SWNTs that were identified as peapods in our studies appeared to be semiconducting, with a gap in the DOS at low voltages. In contrast to unfilled semiconducting SWNTs, peapods exhibit additional electronic features that are strongly dependent on the location along the tube. For example, representative STM tunneling spectra are shown at two different locations spaced 6.3 Å apart along the top of the peapod (Fig. 2). The occupied DOS [voltage ( $V$ ) < 0] of this peapod resembles that of an unfilled semiconducting SWNT; however, the unoccupied DOS contains more complex electronic features, which vary on the nanometer scale. The apparent asymmetry in the STM spectra is consistent with our observation that STM images of peapods are distinct from those of unfilled SWNTs only at positive sample biases.

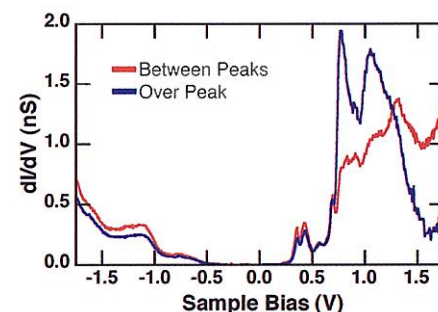


**Fig. 2.** Variation of the DOS in a peapod. A comparison of STM tunneling spectra acquired at 211 Hz, with a 5-mV modulation voltage, is shown. For maximum dynamic range, the STM junction was initially set at +1.75 V and 1.25 nA before sweeping the voltage bias. As a result, the relatively smaller variation in differential conductance ( $dI/dV$ ) observed for negative bias can be attributed to the initial difference in tip heights.

An intensity plot of the spatially resolved STM spectra measured along the peapod axis reveals the modulated electronic structure. For example, in the spectra for a peapod having an ordered array of  $C_{60}$  molecules with a  $9.9 \pm 0.53$  Å spacing (Fig. 3A), although we observe gradual variations of the band structure along the peapod, the most dramatic feature is the periodic spatial variations of its unoccupied DOS. For electron energies above  $\sim 1$  eV, the STM spectra have the expected periodicity of the encapsulated  $C_{60}$  lattice; however, depending on the electron energy, these modulations may be phase-shifted relative to each other by half a period (Fig. 3C). The observation of energy-dependent modulation of the unoccupied DOS is a common characteristic of all ordered peapods in our experiments and is the central experimental finding of this report.

As a final control experiment and to demonstrate directly the importance of the  $C_{60}$  molecules in determining the electronic structure of the peapods, the STM was used to manipulate the encapsulated  $C_{60}$  molecules. Using this technique (21), we have been able to slide the  $C_{60}$  molecules to create unfilled sections in an otherwise filled peapod. We are able, therefore, to compare the spectroscopic measurements performed on the same section of a peapod with and without the encapsulated  $C_{60}$  molecules (Fig. 3, A and D). With the  $C_{60}$  molecules absent (Fig. 3D), the DOS resembles that expected for an unfilled SWNT; however, the presence of the encapsulated molecules results in an apparent rigid shift of  $\sim 60$  meV (Fig. 3B) and in strong modification of unoccupied electronic structure for energies ( $E$ )  $> +1$  eV. This comparison also demonstrates that the gradual spatial variations observed in both spectra are unrelated to the encapsulated molecules and are most likely due to extrinsic effects, such as torsion or strain of the SWNT (22).

To account for our STM measurements of the modulated electronic states in peapods, we first consider the encapsulated  $C_{60}$  molecules. In isolation,  $C_{60}$  has a fivefold degenerate highest occupied  $h_u$  orbital, which is separated by a gap of  $\sim 2$  eV from a threefold degenerate unoccupied  $t_{1u}$  orbital (23). Placed in a close-packed linear array inside a peapod, the dispersion of the  $C_{60}$ -derived band arises from direct overlap between orbitals on nearest neighbor molecules and from an indirect process in which electrons tunnel from a  $C_{60}$  molecule onto the nanotube and then onto a neighboring  $C_{60}$ . The bandwidth for the former direct process can be estimated from the bandwidth of a face-centered-cubic  $C_{60}$  solid, giving a value of  $\sim 100$  meV. This estimate is much smaller than the energy range of the features in our experimental results; hence we conclude that the direct tunneling between the  $C_{60}$  molecules is not as dominant as the indirect tunneling between them through the SWNT. In this

situation, the SWNT acts as a conduit that enhances the coupling between the  $C_{60}$  molecules nested inside of it. Equally important is the periodic arrangement of the  $C_{60}$  molecules, which gives rise to Bragg scattering of the electronic states of the SWNT in a fashion similar to that encountered in the classic 1D Kronig-Penney problem (24).

In constructing a theoretical model, we note that the high symmetries of the electronic states of both SWNTs and  $C_{60}$  molecules constrain their interaction and lead to a simple model for the electronic states of peapods. For a SWNT, the 1D electronic states form a series of occupied and unoccupied energy subbands indexed by the azimuthal quantum number  $m$ . These subbands are arranged symmetrically in energy about the chemical potential, with the  $m = 0, \pm 1$  subbands within a few volts of the chemical potential—near the expected energy range of the  $C_{60}$  molecules' occupied  $h_u$  and unoccupied  $t_{1u}$  orbitals (25, 26). However, the hybridization of SWNT states and the  $C_{60}$  orbitals is strongest for the states with the same azimuthal symmetry. Thus we expect the SWNTs'  $m = 0,$

$\pm 1$  subbands to resonate only with the  $C_{60}$  molecules' unoccupied  $t_{1u}$  "p-like" orbitals and not with the unoccupied  $h_u$  orbitals, which have a "d-like" symmetry. Our experiments confirm this assignment, as they show that occupied states of the peapods are identical to those for unperturbed SWNTs and are insensitive to the encapsulated  $C_{60}$  molecules. We also note that the encapsulation of  $C_{60}$  lifts the degeneracy of its  $t_{1u}$  orbital into an axially oriented  $m = 0$  singlet level and a higher energy  $m = \pm 1$  doublet oriented normal to the SWNT cage. The STM tip couples only to the electronic states that are derived from the mixing of the  $m = \pm 1$   $t_{1u}$  doublet with the SWNT subbands; hence we analyze the data by constructing a theoretical model that hybridizes only these states.

We find that we can understand the differences between the electronic structure of the peapod and that of a SWNT by calculating the band structure for the case of a single  $m = +1$  SWNT subband interacting with a periodic chain of  $C_{60}$   $t_{1u}$  doublet orbitals at  $+1.3$  eV, with spacing  $a = 10$  Å. In making this calculation, we

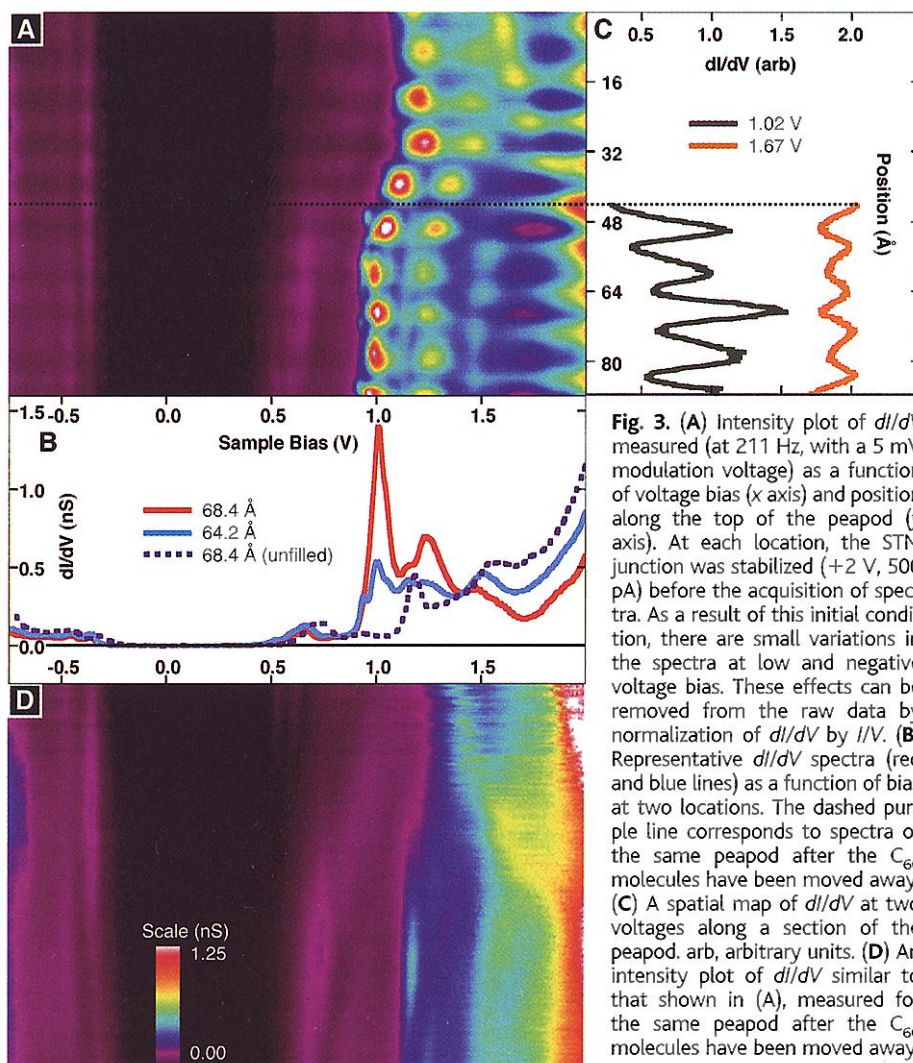


**Fig. 3.** (A) Intensity plot of  $dI/dV$  measured (at 211 Hz, with a 5 mV modulation voltage) as a function of voltage bias (x axis) and position along the top of the peapod (y axis). At each location, the STM junction was stabilized ( $+2$  V, 500 pA) before the acquisition of spectra. As a result of this initial condition, there are small variations in the spectra at low and negative voltage bias. These effects can be removed from the raw data by normalization of  $dI/dV$  by  $I/V$ . (B) Representative  $dI/dV$  spectra (red and blue lines) as a function of bias at two locations. The dashed purple line corresponds to spectra of the same peapod after the  $C_{60}$  molecules have been moved away. (C) A spatial map of  $dI/dV$  at two voltages along a section of the peapod. arb, arbitrary units. (D) An intensity plot of  $dI/dV$  similar to that shown in (A), measured for the same peapod after the  $C_{60}$  molecules have been moved away.

have taken the band edge of the  $m = +1$  subband to be at 1.1 eV, which is the expected value for a semiconducting SWNT having a diameter of 13.1 Å. As shown in Fig. 4A, the model band structure for the peapod is different in two respects from that expected for an unperturbed SWNT. First, the effective coupling between the  $C_{60}$  molecules'  $t_{1u}$  orbitals via the SWNT subband results in the formation of a new narrow band near the energy of the  $t_{1u}$  level. This new band is separated by a hybridization gap from the dispersing  $m = +1$  band of the SWNT, which is shifted up in energy. The periodic potential imposed by the  $C_{60}$  molecules also gives rise to Bragg gaps splitting the SWNT state at the wave vectors  $k = \pm \pi/a$ .

To make a more direct comparison of our model with the measured spectroscopic maps of peapods (Fig. 3), we have calculated the spatial dependence of the DOS as a function of energy (Fig. 4, B and C). The narrow energy band derived from the  $t_{1u}$  orbitals shows strong enhancements in its DOS directly over the  $C_{60}$  molecules at energies close to the edge of the band. This feature of our model calculation and the double peak structure around 1.1 eV in the spectroscopic data of Fig. 3, A and B, is strikingly similar. Furthermore, our calculation shows that the

spatial modulation of the SWNT subband at energies above the hybridization are peaked not over the  $C_{60}$  molecules but rather in between them (Fig. 4C). This phase shift between the electronic states above and below the hybridization gap is also observed in the experimental results, as illustrated in Fig. 3C. Overall, our model calculation captures the salient features of the electronic DOS of the peapods measured in our experiments. Further refinement of this model, such as including the interaction of  $C_{60}$  with other SWNT subbands (such as the lower energy  $m = -1$  subband) and including the spatial extent of  $t_{1u}$  orbitals, can improve the agreement between theory and experiment.

Our theoretical calculation demonstrates how the measured electronic properties of a peapod are different and are derived from those of its constituent parts, but it also provides possible design rules for proposing hybrid structures having a specific type of electronic functionality. At a simple level, as in other heterostructured materials, periodicity imposes important and easily predictable effects on the properties of these systems. However, the role of symmetry of various electronic states (as identified here for a peapod) can perhaps impose less obvious constraints that can be exploited for linking specific electronic states. As the drive toward miniatur-

ization of electronic devices continues, such concepts may be useful in exerting control over selective electronic states in individual nanostructures and for coupling them together.

References and Notes

1. M. S. Dresselhaus, G. Dresselhaus, Ph. Avouris, Eds., *Carbon Nanotubes: Synthesis, Structure, Properties, and Applications* (Springer-Verlag, Berlin, 2001).
2. Z. Yao, H. W. Ch. Postma, L. Balents, C. Dekker, *Nature* **402**, 273 (1999).
3. R. D. Antonov, A. T. Johnson, *Phys. Rev. Lett.* **83**, 3274 (1999).
4. C. Zhou, J. Kong, E. Yenilmez, H. Dai, *Science* **290**, 1552 (2000).
5. S. J. Tans, A. R. M. Verschueren, C. Dekker, *Nature* **393**, 49 (1998).
6. H. W. Ch. Postma, T. Teepen, Z. Yao, M. Grifoni, C. Dekker, *Science* **293**, 76 (2001).
7. T. Rueckes *et al.*, *Science* **289**, 94 (2000).
8. A. Bachtold, P. Hadley, T. Nakanishi, C. Dekker, *Science* **294**, 1317 (2001).
9. V. Derycke, R. Martel, J. Appenzeller, Ph. Avouris, *Nano Lett.* **1**, 453 (2001).
10. P. Nikolaev, A. Thess, A. G. Rinzler, D. T. Colbert, R. E. Smalley, *Chem. Phys. Lett.* **266**, 422 (1997).
11. B. W. Smith, M. Monthieux, D. E. Luzzi, *Nature* **396**, 323 (1998).
12. B. W. Smith, D. E. Luzzi, *Chem. Phys. Lett.* **321**, 169 (2000).
13. K. Hirahara *et al.*, *Phys. Rev. Lett.* **85**, 5384 (2000).
14. B. W. Smith, D. E. Luzzi, Y. Achiba, *Chem. Phys. Lett.* **331**, 137 (1998).
15. K. Suenaga *et al.*, *Science* **290**, 2280 (2000).
16. B. W. Smith, M. Monthieux, D. E. Luzzi, *Chem. Phys. Lett.* **315**, 31 (1999).
17. S. Okada, S. Saito, A. Oshiyama, *Phys. Rev. Lett.* **86**, 3835 (2001).
18. Peapods were synthesized according to recently established high-yield techniques (12) and were ultrasonically agitated in dimethyl formamide to form a dilute suspension. The solution was dripped onto gold-on mica thin film substrates under ambient conditions and dried with nitrogen gas. After introduction into the UHV chamber, the substrates were annealed to remove residual solvent and adsorbed contaminants before cooling to low temperature for measurements.
19. J. W. G. Wildöer, L. C. Venema, A. G. Rinzler, R. E. Smalley, C. Dekker, *Nature* **391**, 59 (1998).
20. T. W. Odom, J.-L. Huang, P. Kim, C. M. Lieber, *Nature* **391**, 62 (1998).
21. D. J. Hornbaker *et al.*, paper presented at the 11th International Conference on Scanning Tunneling Microscopy/Spectroscopy and Related Techniques, Vancouver, British Columbia, 17 July 2001.
22. L. Yang, J. Han, *Phys. Rev. Lett.* **85**, 154 (2000).
23. S. Saito, A. Oshiyama, *Phys. Rev. Lett.* **66**, 2637 (1991).
24. C. Kittel, *Introduction to Solid State Physics* (Wiley, New York, ed. 7, 1996), pp. 180–181.
25. N. Hamada, S. Sawada, A. Oshiyama, *Phys. Rev. Lett.* **68**, 1579 (1992).
26. R. Saito, M. Fujita, G. Dresselhaus, M. S. Dresselhaus, *Appl. Phys. Lett.* **60**, 2204 (1992).
27. Work at the University of Illinois at Urbana-Champaign (A.Y.) was supported under an NSF CAREER Award (DMR-98-75565), by the Department of Energy (DOE) through the Frederick Seitz Materials Research Laboratory (DEFG-02-96ER4539), by the Petroleum Research Fund of the American Chemical Society, and by a Sloan Research Fellowship. Work at the University of Pennsylvania was supported by DOE grant DEFG-02 ER0145118 (E.J.M.); by the Office of Naval Research under grants N00014-00-1-0482 (D.E.L.), DMR 00-7990 (A.T.J.), and DMR 98-02560 (A.T.J.); and through an NSF graduate fellowship (B.W.S.). We thank C. Kane and M. S. Dresselhaus for useful discussions.

16 November 2001; accepted 14 December 2001  
 Published online 3 January 2002;  
 10.1126/science.1068133  
 Include this information when citing this paper.

Fig. 4. Model calculation of the electronic structure of a peapod. The model Hamiltonian used in these calculations has the form

$$H = \frac{1}{a} \int dx \psi^\dagger(x) H_0 \psi(x) + \sum_n \epsilon_n c - c \delta(x - na) [\phi^\dagger(na) \hat{T}^\dagger \cdot \psi(x) + \psi^\dagger(x) \cdot \hat{T} \phi(na)] + \sum_n E_0 \phi^\dagger(na) \phi(na)$$

The first term describes the unperturbed electronic states  $\psi$  of a SWNT subband, in this case an  $m = +1$  subband with a band edge at 1.1 eV. The last term describes the orbital energy of the  $C_{60}$   $t_{1u}$  orbitals, which have an energy  $E_0$  (1.3 eV, blue level in the figure) and are arranged periodically with a spacing  $a = 10$  Å. The second term describes the tunneling between these states, the strength of which is controlled by the matrix elements of the operator  $\hat{T}$ . This coupling is assumed to have strength of 1.25 eV in our calculations. (A) Reduced zone scheme representation of the band structure of a peapod from the model Hamiltonian (solid red line) and that for an unperturbed SWNT with a single subband (dashed line). The hatched regions show the hybridization gap  $\Delta_h$  and the Bragg gap  $\Delta_B$  formed as a result of the coupling of the  $C_{60}$  and the SWNT in the peapods. The wavevector  $k$  in this figure is measured relative to the  $K$  point (Brillouin zone corner) of the graphene sheet. (B) The intensity plot of the spatially resolved DOS as a function of energy ( $x$  axis) and position ( $y$  axis) along the peapod. (C) The DOS over and in between the molecular sites. (D) Spatial dependence of the DOS for energies above and below  $\Delta_h$ , a.u., arbitrary units.

